Journal of the Taiwan Institute of Chemical Engineers 42 (2011) 727–734

Contents lists available at ScienceDirect

Journal of the Taiwan Institute of Chemical Engineers

journal homepage: www.elsevier.com/locate/jtice

Bubble growth for boiling bubbly flow for R141b in a serpentine tube

Mei Huang [a], Zhen Yang [a], Yuan-Yuan Duan [a], Duu-Jong Lee [b,*]

[a] Key Laboratory for Thermal Science and Power Engineering of MOE, Tsinghua University, Beijing 100084, China
[b] Department of Chemical Engineering, National Taiwan University, Taipei 10617, Taiwan

ARTICLE INFO

Article history:
Received 29 October 2010
Received in revised form 31 January 2011
Accepted 28 February 2011
Available online 2 April 2011

Keywords:
Bubbly flow
Secondary flow
Serpentine tube
Bend

ABSTRACT

Bubble growth in flow boiling of R141b in a serpentine tube was experimentally and numerically investigated. Bubble dynamics were recorded and analyzed. Bubbles formed in a straight tube experienced distinct growth phase in the next U-bend: first grew, then shrank and grew again. A single-phase flow simulation was proposed for revealing temperature and flow field in the serpentine tube. The secondary flow at bends twisted the thermal boundary layer and mix cold main stream and superheat boundary layer at wall regime. The effective superheat around the bubble interpreted the bubble behavior noted in experiments.

1. Introduction

U-bends appear widely in pipelines for boilers, heat exchangers and nuclear reactors to change flow router and reduce equipment size. In applications, two-phase flow can occur in the U-bends. Secondary flow occurred in bend flow (both in single and two phases) pushes the fluid to flow in the concave part of the bend (Dean, 1927). Hoang and Davis (1984) detailed structure of bend flow and noted significant pressure drop of two phase flow in two return bends of inner diameter 25.4 mm and curvature ratios of 2 and 3. Other researchers also noted high pressure drops in the bend flow (Kim *et al.*, 1989; Wang *et al.*, 2003).

Traviss and Rohsenow (1973) investigated the pressure drop and flow pattern of two-phase R-12 flows in return bends of inner diameter 8 mm, and curvature ratios 3.17 and 6.35. Usui *et al.* (1980, 1981) experimentally measured the average void fraction and pressure drop in air-water two-phase flows in a vertical C-shaped bend of inner diameter 16 and 24 mm with curvature ratio ranging 11.25–22.5. Flow reversal and flooding were observed due to the gravity-centrifugal force interaction. Chen *et al.* (2002) experimental observed the flow pattern for an air–water two-phase flow in three horizontal bends of inner diameter 6.9 mm and curvature ratio from 3 to 7.1. The two-phase flow pattern in the bends was categorized into five types sequentially along the flow direction; the flow at low mass flux was annular in the recovery region just after the return bend and was then changed to a stratified pattern in the down stream region. The influential length of the downstream straight by the bends of inner diameter 3 and 7 mm was discussed (Wang *et al.*, 2004). Freezing slug flow pattern was observed in a vertical return bend of diameter 6.9 mm but was not noted in tests with diameter of 3 mm (Wang *et al.*, 2008). Meng *et al.* (2009) conducted R141 flow boiling test in hairpin tubes of inner diameter 6 mm. These authors divided bubble dynamics into four regimes based on flow pattern and bubble size.

Unique flow patterns in U-bends lead to distinct heat transfer performance from that in straight pipe. Cho and Tae (2001) reported that heat transfer coefficient in U-bends was higher than that in straight tubes, and the heat transfer coefficient of the downstream straight tube were higher by up to 33% than that of the upstream straight tube. Wen *et al.* (2007) experimentally examined the boiling heat transfer of refrigerant R-600a/R-290-oil mixtures in small-diameter serpentine tubes, and found that the average heat transfer coefficient for serpentine tubes with 2, 4 and 6 bends were 1.05, 1.08 and 1.14 times that of straight pipes. Yang *et al.* (2008) numerically simulated the flow pattern and heat transfer rate for flow boiling of R141b two-phase flow in a serpentine tube. The predicted flow patterns correlated with experimental findings.

Few works have been conducted to observe detailed bubble dynamics in flow boiling in U-bends. This work aims at observing bubble behaviors in a boiling bubbly flow for R141b in a serpentine tube with three bends. A computational fluid dynamic (CFD) model was adopted to simulate flow patterns and heat transfer characteristics in U-bends. Correlation between local superheat and bubble growth rate was discussed.

2. Experimental

2.1. Experiment system

Fig. 1(a) schematically shows the experiment setup, consisting of liquid tank (1), pump (2), flow meter (3), pre-heater (4), pre-

* Corresponding author. Fax: +886 2 2362 3040.
E-mail addresses: djlee@ntu.edu.tw, djleetw@yahoo.com (D.-J. Lee).

1876-1070/$ – see front matter © 2011 Taiwan Institute of Chemical Engineers. Published by Elsevier B.V. All rights reserved.
doi:10.1016/j.jtice.2011.02.007

Nomenclatures

C_p	liquid specific heat (J/kg-K)
$\vec{G}$	non-dimensional gravity vector, $\vec{G} = \vec{g}/(\rho_l u_0^2)$
$\vec{g}$	gravity vector (m^2/s)
$\vec{i}$	unit vector in the x-direction
$\vec{j}$	unit vector in the y-direction
$\vec{k}$	unit vector in the z-direction
P	non-dimensional pressure $P = p/(\rho_l u_0^2)$
Pr	Prandtl number
p	pressure (Pa)
Q_m	mass flow rate (kg/s)
q''	wall heat flux (W/m)
R_0	tube radius (m)
Re	Reynolds number, $Re = (\rho_l u_0 R_0)/\mu_l$
U	non-dimensional velocity, $U = u/u_0$
T	temperature (K)
T_s	saturation temperature (K)
u_0	mean velocity at the tube inlet
X	non-dimensional x coordinate
x	x coordinate
Y	non-dimensional y coordinate
y	y coordinate
Z	non-dimensional z coordinate
z	z coordinate

Greek symbols

ρ_l	liquid density (kg/m)
ρ_v	vapor density (kg/m)
θ	non-dimensional temperature, $\theta = k(T - T_s)/(q''R_0)$

mixing chamber (5), test section (6), post-mixing chamber (7), filter (8), condenser (9), CCD camera (10), personal computer (11) and circuit controller (12). A working liquid R141b was pumped through the tank, flow meter, pre-heater, pre-mixing chamber, test tube, post-mixing chamber, filter and condenser. The serpentine tube, 4 mm in inner diameter and 6 mm in outer diameter, was made of smooth quartz glass tube with three turns and was placed horizontally (Fig. 1(b)). The turning radii of the return bends were 12.5 mm. The serpentine tube was connected to copper tubes with corrosion-resistant sealant. The outer surface of the tube was coated with a transparent metal oxide thin film which was electrically conductive and was used for Joule heating. By charging a direct-current (DC) power between the electric poles, a uniform heat flux was applied to the outer surface of the tube.

2.2. Tests and measurements

Experiment was conducted by first pumping liquid over test section with no heat input. Then, the DC power was on at prescribed voltage. Experimental measurements for flowrate, temperature and pressure were made using flowmeter (LZB-6, Funyo, Co., Zhejiang, China), resistance temperature detectors (Pt-100, ZIEHL, Daimlerstraße, Germany) and pressure transmitter (JYB-KO-PAA-1Z, ColliHigh, Beijing, China), respectively. The liquid sub-cooling at tube inlet was 10 K. The local pressures were measured by sensors and their values were maintained at 100 kPa and 114 kPa at inlet and outlet of the serpentine tube. The relative uncertainties of experimental measurements were ±2.5%, ±0.37% and ±2.5% for flowrate, temperature and pressure, respectively.

Natural heat transfer loss form the test section was evaluated. The natural convection heat transfer coefficient h_0 is commonly lower than 10 W/m/K. Seven thermocouples were attached to different locations on the top surface of the outer wall of the tube, as seen in Fig. 1(b). The average temperature T_w measured was used to estimate the heat loss by natural convection. For instance, at a mass flux of Q_m = 136 kg/m/s and a heat flux of q'' = 5810 W/m, the obtained T_w was 59.1 K, resulting in a heat loss of 2.34 W estimated by $h_0 A(T_w - T_0)$, where T_0 is the room temperature (~20 K) and A = 6054.6 mm^2 the area of the tube outer wall. The heat loss was relatively low compared to the heating power 34.9 W. In other case studied, the heat loss did not exceed 8% of the heating power.

The boiling bubbly flow in the tube was observed and recorded by a high-speed CCD camera at 500 fps and resolution of 0.1 mm/pixel, with images sent to a computer for analysis. A detailed description of the test apparatus can be found elsewhere (Lin *et al.*, 2003).

3. Numerical simulation

3.1. Model description

Bubbly flow has recently been numerically simulated (Dong and Yu, 2009; Rabha and Buwa, 2010; Selma *et al.*, 2010; Wu and Lu, 2002). However, comprehensive numerical simulation of bubbly flow in a boiling process is still a challenging task. The present study conducted simplified, single-phase model for simulation the case with bubble inception. When bubble volume fraction is relatively low, e.g., <5% of the total fluid volume, the bubble impacts on the surrounding flows are limited and the flow and heat transfer could be close to that without bubbles. Therefore,

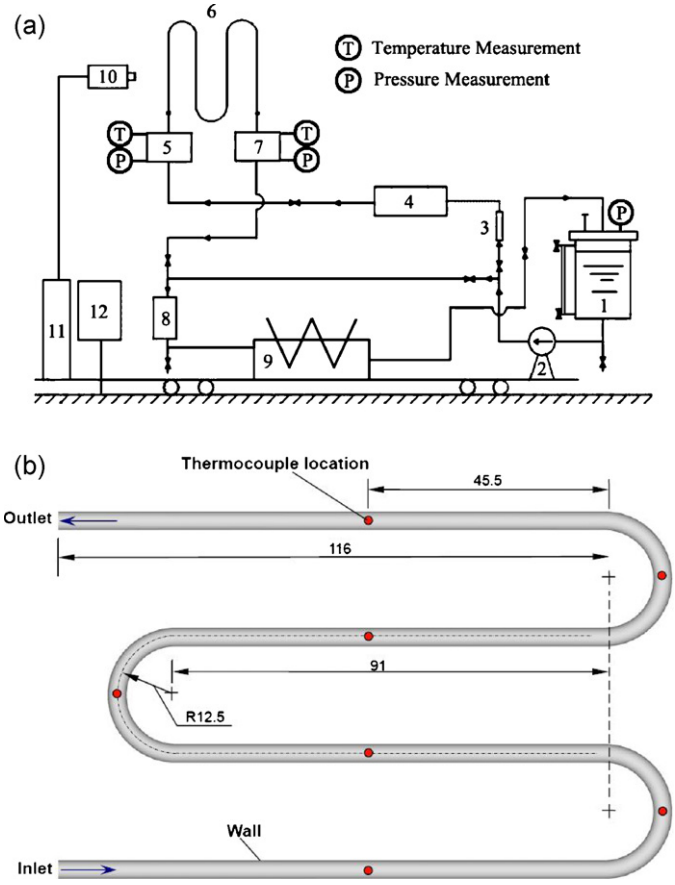

Fig. 1. Experimental system (a) and test section (b): (1) tank; (2) pump; (3) flow meter; (4) pre-heater; (5) pre-mixing chamber; (6) test section; (7) post-mixing chamber; (8)filter; (9) condenser; (10) CCD; (11) computer; (12) circuit controller.

using a single-phase model for simulation may still be able to conserve the main features of bubbly flow in terms of the flow and heat transfer in the surrounding fluid. As shown in the next sections, the simplified model can effectively reveal the flow details and reasonably elucidate the experimental observations for boiling in U-bends.

The Reynolds number in this study is lower than the critical value for the laminar-turbulent transition in U-bends, for example, 7800 at curvature ratio of 7 (Soh and Berger, 1984). Therefore, a three-dimensional incompressible laminar flow and heat transfer model was adopted for simulation. The non-dimensional governing equations, i.e., continuum, momentum and energy equations are listed as follows.

$$\nabla \cdot \vec{U} = 0 \tag{1}$$

$$\vec{U} \cdot \nabla \vec{U} = \frac{1}{Re} \nabla^2 \vec{U} - \nabla P + \vec{G} \tag{2}$$

$$\vec{U} \cdot \nabla \theta = \frac{1}{RePr} \nabla^2 \theta \tag{3}$$

where the mathematic operator ∇ is written as $\nabla = \vec{i}(\partial/\partial X) + \vec{j}(\partial/\partial Y) + \vec{k}(\partial/\partial Z)$.

The computational domain with hexahedral grids generated using GAMBIT 2.3.16 (ANSYS, Inc., Ann Arbor, MI, USA) (Fig. 1(b)) was the same as the flow channel used in the experiments. Flow dependency on meshing was checked by conducting simulations using different grid numbers. The final grid used for calculation had more than 400,000 elements.

Fully developed conditions were applied at the inlet of the tube, i.e.,

$$\vec{U} = 2(1 - R^2)\vec{i} \tag{4}$$

and

$$\theta = R^2 - \frac{R^4}{4} - \frac{7}{48} + S_0 \tag{5}$$

where R is a non-dimensional radius defined as $R = r/R_0$, and S_0 is the non-dimensional form of the inlet average subcooling. When $S_0 = 0$, the fluid is at saturation in terms of flow-averaged temperature, and fluid is sucooled/supheated at $S_0 < 0/S_0 > 0$.

At the tube outlet, $80R_0$ away from the last bend, the flow field has minimal influence on upstream condition, with

$$\frac{\partial \vec{U}}{\partial X} = 0, \quad \frac{\partial \theta}{\partial X} = 0 \tag{6}$$

At tube wall, no-slip flow boundary condition and constant heat flux boundary condition were applied:

$$\vec{U} = 0, \quad \frac{\partial \theta}{\partial \vec{n}} = 1 \tag{7}$$

where $\vec{n}$ is the unit vector normal to the wall.

3.2. Numerical methods

Values at the centers of the hexahedral cells were stored for all variables including velocity, pressure and temperature. A second-order upwind scheme was used for convective flux, while a central-differencing scheme was used for discretizing the diffusion flux.

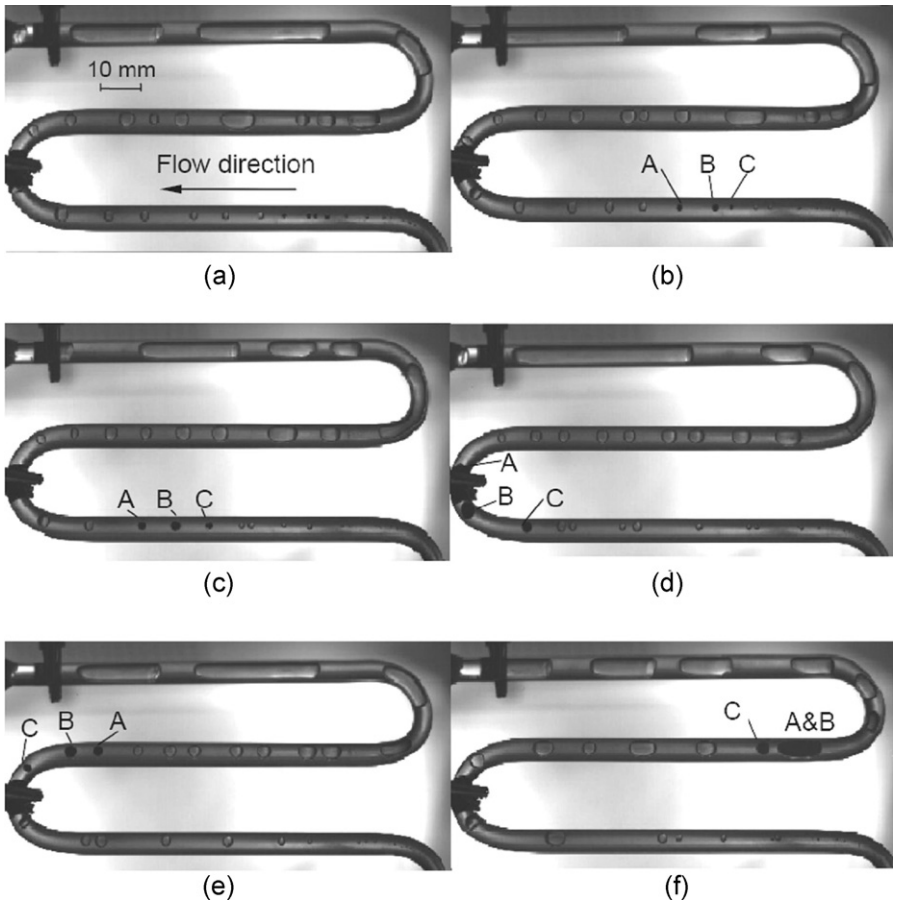

Fig. 2. Bubble stream at Q_m = 136.0 kg m/s and q'' = 5810 W/m: (a) t = 0 ms, (b) t = 160 ms, (c) t = 400 ms, (d) t = 720 ms, (e) t = 940 ms, (f) t = 1620 ms.

The pressure–velocity coupling was implemented via the PISO algorithm (Issa, 1986). Iterations at each time step were terminated when the dimensionless residuals for all equations were below 10^{-4}. The computation was performed using the commercial software FLUENT 6.1 (ANSYS Inc., Ann Arbor, MI, USA) (Fluent, 2003).

4. Results and discussion

4.1. Bubble visualization

Figs. 2 and 3 present the flow patterns at Q_m = 136 kg m/s and q'' = 5810 W/m, and Q_m = 204 kg m/s and q'' = 8720 W/m, respectively. Flowrate and heat flux were selected to have bubble inception point near the entry of the first straight tube and develop a bubbly flow through most parts of the flow path. The subcooling at entry ranged 9.0–9.8 K.

A typical test in Fig. 2 revealed three small bubbles (case 1), i.e., A, B and C, generated in the second straight tube at t = 160 ms and steadily grew in size in the straight section at t = 400 ms before entering the bend at t = 720 ms. In the bend bubble size decreased, as seen from the comparison of bubble C between Fig. 2(d) and (e). Similar phenomenon was observed in other tests (see Fig. 3, case 2). Due to action of gravity, formed bubbles moved close to the inner top surface of the tube.

The subcooling S at the entrance of the second bend can be calculated as follows.

$$S = S_0 + \frac{q'' \cdot (A_{s1} + A_{s2} + A_{b2})}{Q_m C_p} \quad (8)$$

where A_{s1}, A_{s2} and A_{b2} are the inner wall areas of the first, second straight tubes and the first bend. The calculated subcooling at the inlet of the second bend is 0.78 K and −0.2 K in case 1 and case 2, respectively.

Fig. 4 presents the time evolutions of bubble projected area in images acquired by CCD camera. The bubble area increased when passing through the second straight tube. As the bubble entered the second bend (the blank symbol section on the left part of each curve), its projected area first grew, then shrunk and finally grew again over time. As bubble flew into the third straight tube (solid symbols), steady growth of bubble area was noted. The steady growth persisted at the third bend and the fourth straight tube section. The abrupt growth of bubble A in case 1 at around 1500 ms was caused by its coalescence with a nearby bubble.

4.2. Temperature profile and flow field: simulation

Fig. 5 shows the simulation results for superheat ($T - T_s$) profile on the vertical center plane of the serpentine tube. The negative-superheat regions represent subcooled zones while those in positive regions are superheated zones. In the second straight tube regime, although the main stream at the tube center has a subcooling of 2–4 K, a superheated thermal layer has already been built up in the tube wall regions. When a bubble was attached to the top inner wall of the tube, it resided in the superheat thermal layer.

Fig. 6 shows the flow streamlines and the resulting temperature field in the second bend. The temperature profiles in the bends were apparently different from the straight tubes. The flow streamlines in the second straight tube, i.e., before Section A, were a set of straight lines. Hence, the fluid elements in the wall region were remained in the thermal layer regime to accumulate heat. As the flow enters the bend, the flow streamlines were twisted by centrifugal force. The superheated fluid elements no longer stayed

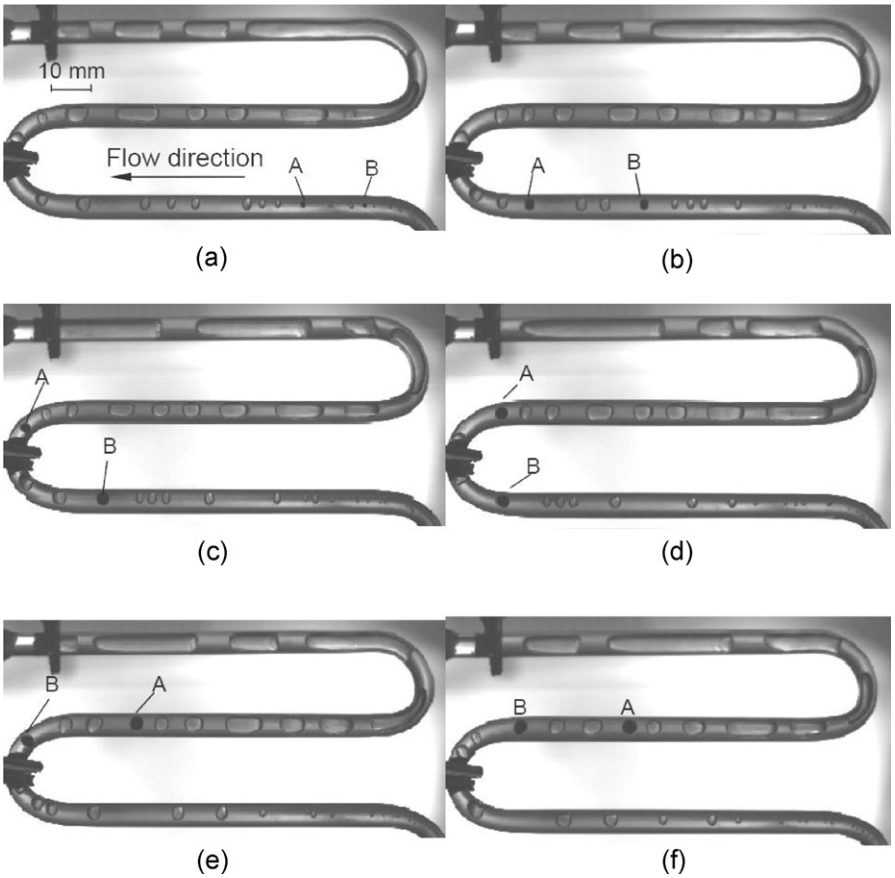

Fig. 3. Bubble stream at Q_m = 204.0 kg/m/s and q'' = 8720 W/m: (a) t = 0 ms, (b) t = 400 ms, (c) t = 560 ms, (d) t = 620 ms, (e) t = 740 ms, (f) t = 820 ms.

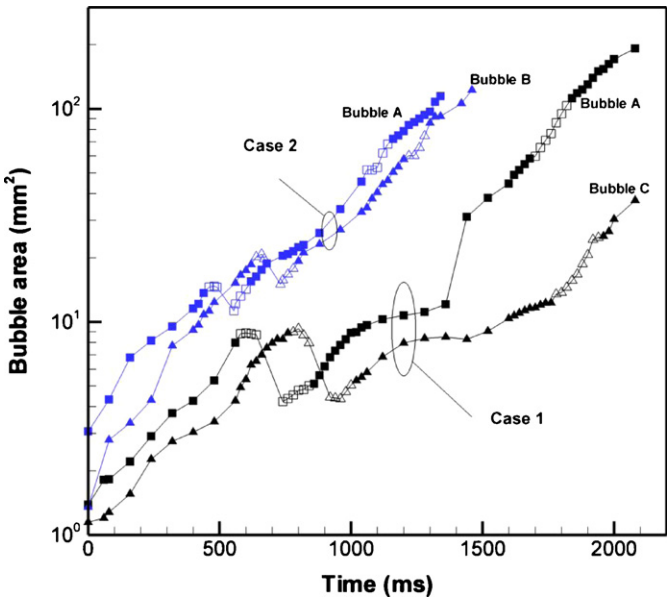

Fig. 4. Bubble area variations. The solid symbols represent bubble growth sequentially in the second, third and fourth straight tubes and the blank ones are for the second and third bends. The starting points correspond to the images at $t = 0$ ms in Figs. 2 and 3.

in the wall boundary region; instead, they flew to the center regions of the tube, as shown by streamlines a, b, c and d. The mixing effects by secondary flow reduced local superheat at the wall regions of the bend. The secondary flow-induced temperature profile could be responsible for the growth singularity of bend bubbles observed in the experiments.

4.3. Bubble growth

Evaporation can take place in some parts of the bubble surface with positive interfacial superheat while condensation can occur in other parts with negative interfacial superheat. Whether a bubble grows depends on the overall mass flux on its interface: it grows with a positive overall mass flux and shrinks with a negative flux.

According to the classical bubble dynamic models, the vapor temperature T_v inside the bubble is obtained from the Laplace and Clausius–Clapeyron equations,

$$T_v = T_s + \frac{2\sigma T_s}{h_{lv}\rho_v r_b} \tag{9}$$

where h_{lv} the potential enthalpy, σ the surface tension, and r_b the bubble radius. Consider the small bubble size (about 1.5 mm) implemented in the tests, Eq. (9) can be simplified following assumption made by (Wang *et al.*, 2005).

$$T_v \approx T_s \tag{10}$$

The phase-change heat transfer at the interface is calculated as follows:

$$q'' = h_i(T_i - T_v) \tag{11}$$

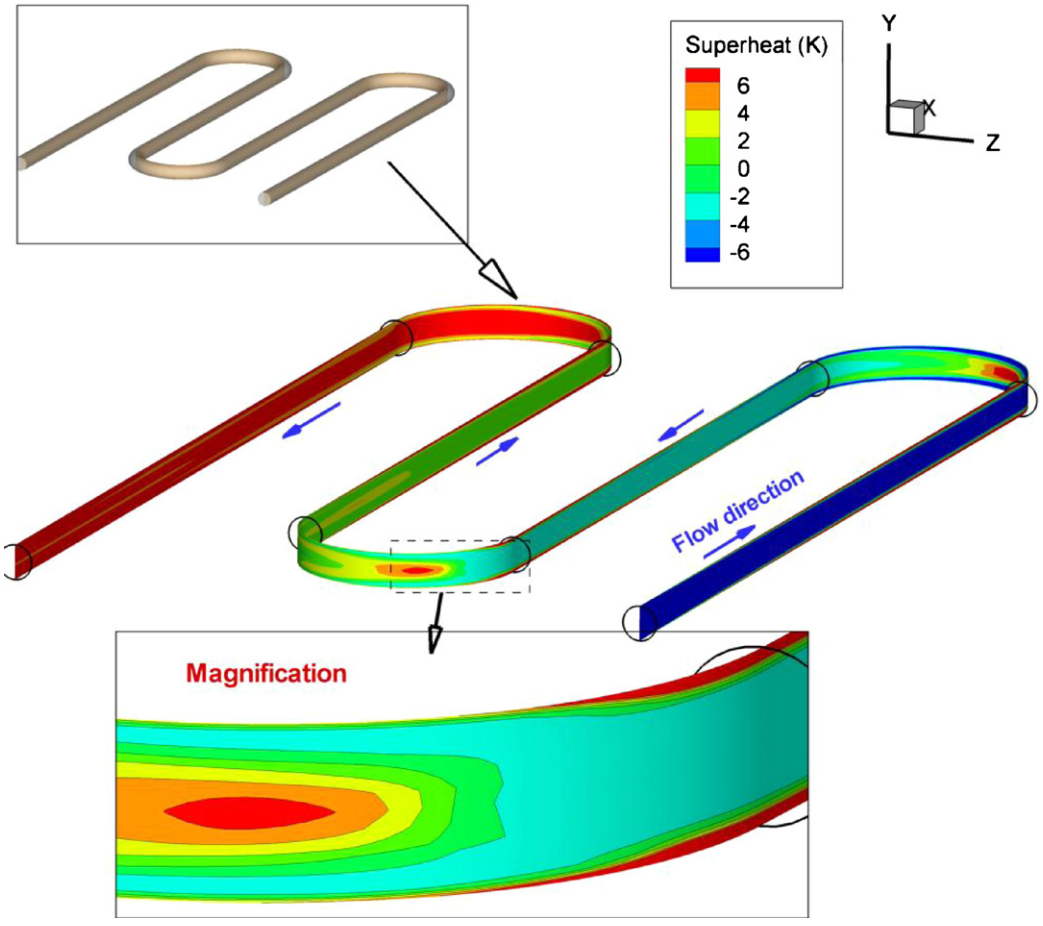

Fig. 5. Temperature field on the vertical center plane of the serpentine tube.

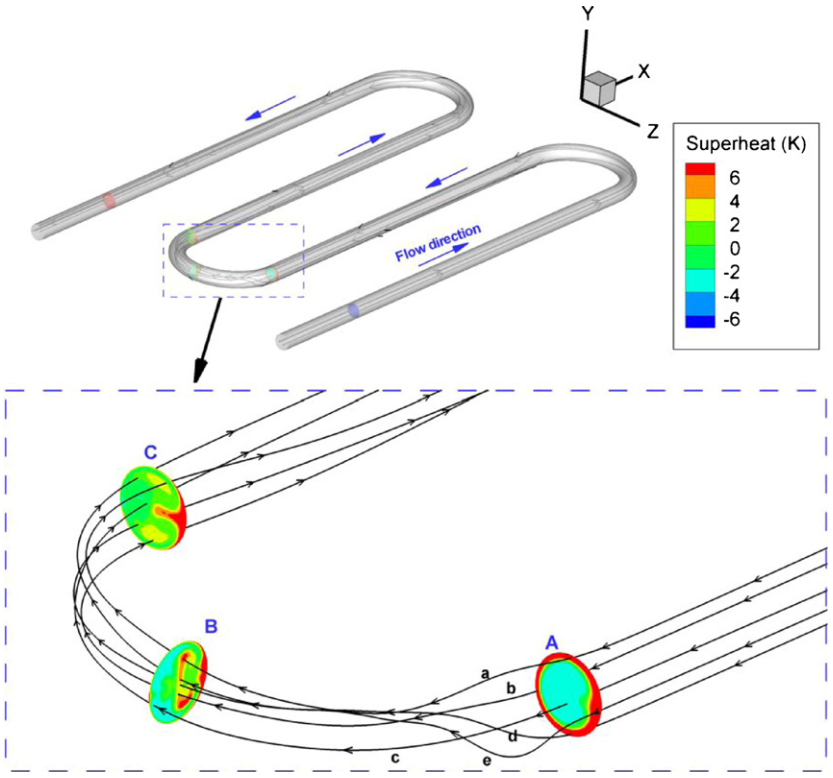

Fig. 6. Flow streamlines through the tube and temperature profiles on three cross-sections in the second bend.

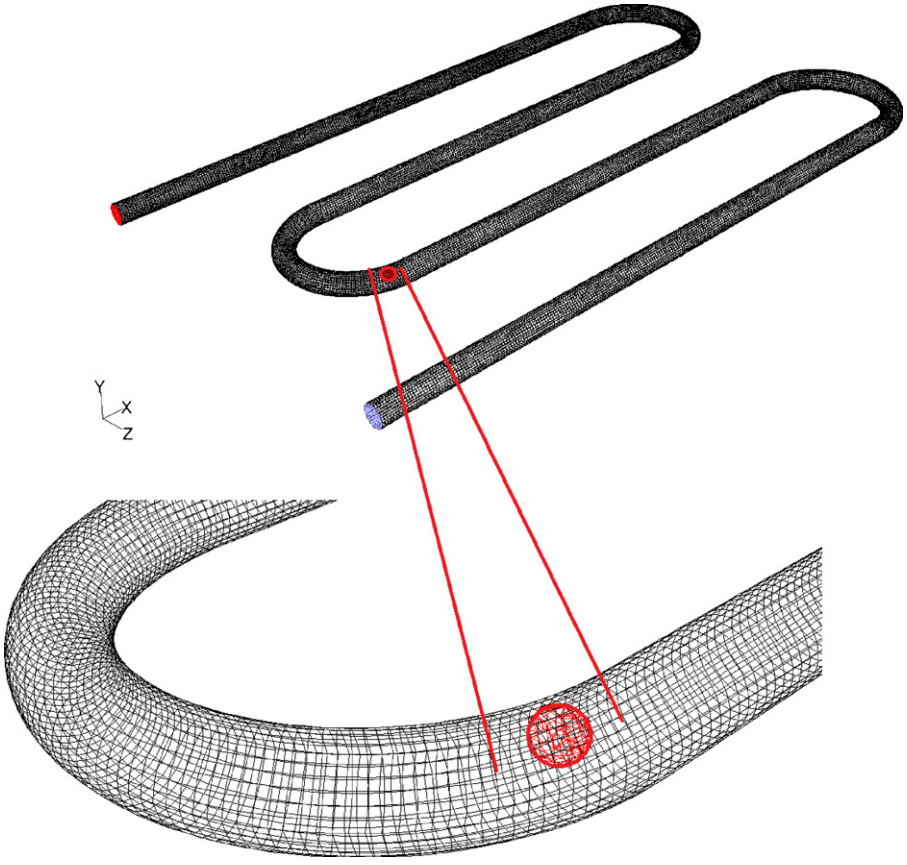

Fig. 7. Spheres constructed in FLUENT as bubbles in the tube.

where h_i is the heat transfer coefficient at the bubble interface (Carey, 1992):

$$h_i = \left[\frac{2\hat{\sigma}}{2-\hat{\sigma}}\right]\left(\frac{\rho_v h_{lv}^2}{T_v}\right)\left(\frac{\bar{M}}{2\pi\bar{R}T_v}\right)^{0.5}\left(1-\frac{p_v}{2\rho_v h_{lv}}\right) \quad (12)$$

where $\hat{\sigma}$ is accommodation coefficient, $\bar{M}$ molar mass, $\bar{R}$ the molar gas constant and ρ_v vapor density. Paul (1962) claimed that the accommodation coefficient of water is $\hat{\sigma} = 0.02-0.04$. As the dipole moment of R141b molecule is 2.0D, very close to that of water, $\hat{\sigma}$ of R141b is taken as 0.03. Since h_i is of order 10^5–10^6, liquid superheat principally determines bubble growth rate, hence minimizing possible errors introduced by set parameter $\hat{\sigma}$ value.

The bubble growth is determined by the overall mass flux Q'' at the interface, which is an integration of mass flux over the interface:

$$Q'' = \int_{\text{interface}\,A} q''\,dA \quad (13)$$

The growth rate of bubble is measured by the temporal change in its radius as follows:

$$\frac{dr_b}{dt} = \frac{Q''}{4\pi r_b^2 \rho_v h_{lg}} \quad (14)$$

From the above equation, bubble radius increases if Q'' is positive and decreases on the contrary. Q'' depends on the local heat transfer rate which is calculated by the temperature field around the bubble.

A spherical regime was defined in the calculated thermal field with position, as shown in Fig. 7, and radius of the bubble identical as that noted in experiments so the local temperature distribution on the spherical "surfaces" of bubble can be obtained. From the surface temperature distribution a preliminary estimate of bubble growth rate can be conducted based on Eqs. (13) and (14) (Fig. 8). The bubble areas in experiments were measured by first detecting edges of bubbles using the Sobel method in MATLAB 2007b (MathWorks Inc., Natick, MA, USA) image processing toolbox, then manually accounting the pixel number in the enclosed bubble edges and multiplying the number with the square of pixel size, while those in simulations were calculated by πr_b^2.

By calculation, a "virtue" bubble (Fig. 7) passing through the second bend would first slightly grow in the first one third of bend (0–60°), then shrink in the middle portion (60–120°), and finally grow again in the last one third of bend (120–180°), qualitatively correlating with the observation (Fig. 4). Conversely, the virtue bubble would grow continuously in the 3rd bend, unlike that for the 2nd bend. Such an observation is owing to the difference in superheat for the 2nd and the 3rd bends: −4 to −2 K for the former, and 0–2 K for the latter. In the third bend, the simulation deviates from experimental observations: the bubble sizes predicted at the end of the bend (180°) were almost 10 times the experimental values. However, both approaches were consistent in terms of the growth trend.

The reason why the predicted bubble growth in the third bend was much faster than that in the experiments is as follows. The simulations here was designed for slow bubble growth with the bubble impacts on flow and heat transfer being safely negligible, which was true with the initial bubble growth at the second bend where the fluid was subcooled and bubble growth was slow. As the bubble entered into the third bend bubble growth rate was increased due to an increase in the fluid temperature, and the impact of bubble on heat transfer became relatively important. Since the current simulation did not account for the bubble impacts, it neglected the cooling effect of bubble growth on the fluid and, as a result, the fluid temperature was over predicted, which led to the falsely faster growth of bubbles.

4.4. Superheat effect

It is known from section *Bubble growth* that local superheat significantly affects bubble growth at bends. Fig. 9 shows the simulated growth rates for two bubbles in the bend with different superheats at the bend inlet. The bubbles would decrease in size at a negative superheat of −0.1 K; while they would increase in size at a positive superheat of 0.1 K. Additionally, over the first part of the bend (0–20°), the 0.5-mm-radius bubble can grow even at a −0.1 K superheat, unlike what happens for the 1-mm-radius bubble case during which bubble shrinks in size. This is because a large part of the 0.5 mm bubble is in the thermal boundary layer at the early part of the bend and evaporation at the interface sustains the

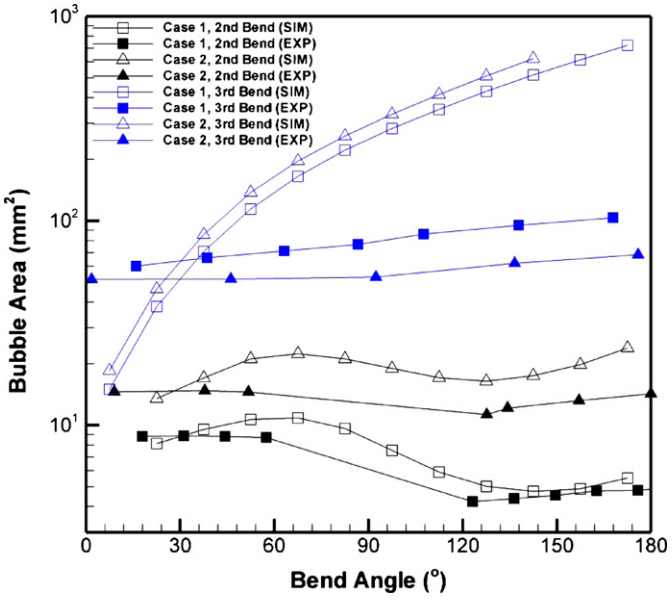

Fig. 8. Comparison of bubble growth (Bubble A in Figs. 2 and 3) between simulations (SIM) and experiments (EXP).

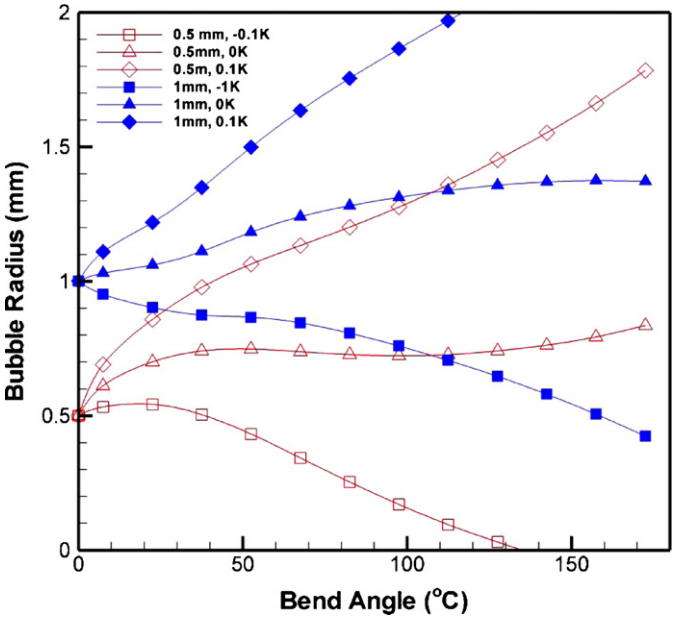

Fig. 9. Simulated growth for two bubbles (of 0.5 and 1 mm in the initial radius) at the bend at different inlet superheats (Q_m = 125 kg/m/s, q'' = 50 W/m).

bubble growth; however, the 1 mm bubble has a large part of interface in contact with the cool main stream and condensation at the interface results in bubble shrinkage. In the experiments, bubbles at the 2nd bend had sizes of 2–3 mm, larger than those in Fig. 9, indicating the cool main stream can greatly affect the bubbles and reduce their sizes. This is why bubble size reductions were typically seen in the 2nd bend in the experiment and the related simulations (Figs. 4 and 6), but not in Fig. 9. The non-uniformity of temperature field is mainly responsible for the unique bubble growth noticed here, which is quite different from the case of pool boiling, where the mainly stream temperature is relatively uniform, and bubble growth rate is monotonically increased with the superheat (Siedel *et al.*, 2008).

5. Conclusions

Experiments were carried out to monitor bubble dynamics during boiling bubbly flow of R141b in a serpentine tube. A simplified single-phase CFD model was developed to interpret the combined effects of flow field and heat transfer on bubble growth. In the straight tube sections, bubbles attached to the top inner tube wall would grow steadily; in the bend regime with a subcooled main stream flow, bubbles would first grow, then shrink and then grow again; in the bend with superheated fluid flow, all bubbles would grow steadily and consequently turn into slugs.

The secondary flow at the bends twisted the superheat boundary layer at wall regime, leading to reduction in superheat around growing bubble. The simulated bubble growth rate correlated with experimental observations at the 2nd bend with subcooled main stream; however, deviation was noticed at the 3rd bend with superheated main stream. The bubble behavior is well interpreted by the effective superheat noted in the different flow regimes.

Acknowledgements

The authors thank the National Natural Science Founding of China (Grant Nos. U0934006 and 50976054) for the financial support to this work.

References

Carey, V. P., *Liquid–Vapor Phase-change Phenomena*, Hemisphere, Washington, DC, USA (1992).

Chen, I. Y., Y. M. Yang, and C. C. Wang, "Influence of Horizontal Return Bend on the Two-phase Flow Pattern in a 6.9-mm Diameter Tube," *Can. J. Chem. Eng.*, **80**, 478 (2002).

Cho, K. and S. J. Tae, "Condensation Heat Transfer for R-22 and R-407C Refrigerant-oil Mixtures in a Micro-fin Tube with a U-bend," *Int. J. Heat Mass Transfer*, **44**, 2043 (2001).

Dean, W. R., "Note on The Motion of Fluid in Curved Pipe," *Philos. Mag.*, **4**, 208 (1927).

Dong, X. F. and A. B. Yu, "Numerical Analysis of the Heterogeneous Gas–Solid Flow in Fluidized Beds," *J. Taiwan Inst. Chem. Engrs.*, **40**, 645 (2009).

Fluent, In c., *FLUENT 6. 1 Documentation.* , Fluent, Inc., http://www.fluent.com/ ().

Hoang, K. and M. R. Davis, "Flow Structure and Pressure Loss for Two-phase Flow in Return Bends," *J. Fluids Eng.*, **106** (1984).

Issa, R. I., "Solution of Implicitly Discretized Fluid Flow Equations by Operator Splitting," *J. Comput. Phys.*, **62** (1986).

Kim, J. S., N. Katsuya, K. Masafumi, K. Kouichrio, and H. Toshiaki, "Influence of Oil on Refrigerant Evaporator Performance—4th Report: Flow Regime and Pressure Drop in Return Bend," *Trans. JAR*, **6**, 79 (1989).

Lin, T. J., P. C. Chen, and H. T. Chiu, "Experimental Measurements and Numerical Simulation of the Hydrodynamics in an Airlift Reactor: Dispersed Bubbling Regime," *J. Chin. Inst. Chem. Engrs.*, **34**, 497 (2003).

Meng, M., X. F. Peng, P. Ye, and Y. Y. Duan, "Bubble Dynamical Behavior and Thermal Non-equilibrium during Flow Boiling in U-turn Bends of Hairpin Tubes," *Chem. Eng. Process.*, **48**, 1177 (2009).

Paul, B., "Complication of Evaporation Coefficient," *ARS J.*, **32**, 1321 (1962).

Rabha, S. S. and V. V. Buwa, "Volume-of-fluid (VOF) Simulations of Rise of Single/multiple Bubbles in Sheared Liquids," *Chem. Eng. Sci.*, **65**, 527 (2010).

Selma, B., R. Bannari, and P. Proulx, "Simulation of Bubbly Flows: Comparison between Direct Quadrature Method of Moments (DQMOM) and Method of Classes (CM)," *Chem. Eng. Sci.*, **65**, 1925 (2010).

Siedel, S., S. Cioulachtjian, and J. Bonjour, "Experimental Analysis of Bubble Growth, Departure and Interactions during Pool Boiling on Artificial Nucleation Sites," *Exp. Thermal Fluid Sci.*, **32**, 1504 (2008).

Soh, W. Y. and S. A. Berger, "Laminar Entrance Flow in a Curved Pipe," *J. Fluid Mech.*, **148**, 109 (1984).

Traviss, D. P. and W. M. Rohsenow, "The Influence of Return Bends on the 344 Downstream Pressure Drop and Condensation Heat Transfer in Tubes," In: ASHRAE Semiannual Meeting. II, No. 2269RP-63 (1973).

Usui, K., S. Aoki, and A. Inoue, "Flow Behaviour and Pressure Drop of Two-phase Flow through C-shaped Bend in Vertical Plane, (I) Upward Flow," *J. Nucl. Sci. Technol.*, **17**, 875 (1980).

Usui, K., S. Aoki, and A. Inoue, "Flow Behaviour and Pressure Drop of Two-phase Flow through C-shaped Bend in Vertical Plane, (II) Downward Flow," *J. Nucl. Sci. Technol.*, **18**, 179 (1981).

Wang, C. C., I. Y. Chen, and H. J. Shyu, "Frictional Performance of R-22 and R-410a Inside a 5.0 mm Wavy Diameter Tube," *Int. J. Heat Mass Transfer*, **46**, 755 (2003).

Wang, C. C., I. Y. Chen, Y. W. Yang, and R. Hu, "Influence of Horizontal Return Bend on the Two-phase Flow Pattern in Small Diameter Tubes," *Exp. Thermal Fluid Sci.*, **28**, 145 (2004).

Wang, C. C., I. Y. Chen, Y. T. Lin, and Y. J. Chang, "A Visual Observation of the Air–Water Two-phase Flow in Small Diameter Tubes Subject to the Influence of Vertical Return Bends," *Chem. Eng. Res. Des.*, **86**, 1223 (2008).

Wang, H., X. F. Peng, D. M. Christopher, W. K. Lin, and C. Pan, "Investigation of Bubble-top Jet Flow during Subcooled Boiling on Wires," *Int. J. Heat Fluid Flow*, **26**, 485 (2005).

Wen, M. Y., C. Y. Ho, and J. K. Jang, "Boiling Heat Transfer of Refrigerant R-600a/R-290-oil Mixtures in the Serpentine Small-diameter U-tubes," *Appl. Thermal Eng.*, **27**, 2353 (2007).

Wu, H. Z. and W. M. Lu, "Numerical Estimation of Local Gas Holdup in Gas–Liquid Contactors," *J. Chin. Inst. Chem. Engrs.*, **33**, 429 (2002).

Yang, Z., X. F. Peng, and P. Ye, "Numerical and Experimental Investigation of Two Phase Flow during Boiling in a Coiled Tube," *Int. J. Heat Mass Transfer*, **51**, 1003 (2008).